Supporting Information

Schroeder et al. 10.1073/pnas.1213471110

SI Materials and Methods

Wavelength Settings. Auto-fluorescence: excitation (exc) 340 nm, emission (em) >480 nm. JC-1 (10 min loading with 5 μM): exc 488 nm, em 580 nm/525 nm. Tetramethylrhodamine ethyl ester (TMRE; 5 min loading with 10 μM): exc 555 nm, em >600nm. Mag-Indo1 (10 min AM-loading with 10 μM): exc 361 nm, em 475 nm/400 nm. cSNARF-1 (myocytes: 10–60 min AM-loading with 10 μM; longer loading-times favored greater partitioning into mitochondria; isolated mitochondria: 30 min AM-loading with 50 μM): exc 555 nm (confocal) or 488 nm (flow cytometer), em 580 nm/640 nm. BCECF (30 min AM-loading with 20 μM): alternating exc 440/495 nm, em 525 nm. BCECF and cSNARF-1 ratios were calibrated by the nigericin technique (1). DHPE-fluorescein (DHPE-F; mitochondrial colocalization experiments: 90 s exposure to 1 mM; intermembrane space (IMS) measurements: 10 min loading with 10 μM): alternating exc 405/488 nm, em >520 nm. Also see ref. 2 for details of the loading procedure with phospholipid-tagged fluorescein derivatives. Wheat germ agglutinin (WGA)-fluorescein (10 min loading with 10 μM): alternating exc 405/488 nm, em >520 nm (correction for auto-fluorescence: determined as the *x*-axis intercept of the plot of 405 nm- vs. 488 nm-excited fluorescence under constant pH). DHPE- and WGA-fluorescein ratios were calibrated to pH by exposure to a highly buffered solution of fixed pH without respiratory substrates. Alexa Fluor 555: exc 555 nm, em >560 nm.

Preparation of Hyperpolarized [1-^{13}C]Pyruvate. [1-^{13}C]Pyruvic acid was prepared and polarized in a ^{13}C polarizer system (Oxford Instruments) (3) with 15 mM OX063 and a trace amount of the gadolinium compound 1,3,5-Tris-(*N*-(DO3A-acetamido)-*N*-methyl-4-amino-2-methylphenyl)-[1,3,5]triazinane-2,4,6-trione, referred to here as "3-Gd." The [1-^{13}C]pyruvic acid and trityl radical OX063 were obtained from GE Healthcare (Amersham), and 3-Gd was obtained from Imagnia AB. [1-^{13}C]Pyruvate was generated via dissolution of the [1-^{13}C]pyruvic acid in hyperpolarized ^{13}C dissolution buffer (13CB) after >45 min to allow nuclear polarization to build up.

In Vivo Hyperpolarized ^{13}C Magnetic Resonance Spectroscopy on Anesthetized Rats. A home-built ^{1}H/^{13}C butterfly coil was placed over the rat's chest, localizing signal from the heart. Rats were anesthetized and monitored as described previously (3) and positioned in a 7-T horizontal-bore MR scanner interfaced to a Varian Inova console (Varian Medical Systems). Correct positioning was confirmed by the acquisition of an axial proton image. An ECG-gated shim was used to reduce the proton line width to ∼120 Hz. Immediately before infusion, an ECG-gated ^{13}C-MR pulse-acquire spectroscopy sequence was initiated. One milliliter of hyperpolarized pyruvate was infused over 10 s into the anesthetized rat. Thirty individual cardiac spectra were acquired over 1 min following infusion (2-s temporal resolution; 7.5° excitation flip angle; 180 parts per million (ppm) sweep width; 4,096 acquired points; frequency centered at 125 ppm). Resonances corresponding with the cardiac $H^{13}CO_3^-$ and $^{13}CO_2$ resonances were located at 161 and 125 ppm, respectively.

Ex Vivo Experiments on Perfused Hearts. ***Preparation for Langendorff perfusion.*** Male Wistar rats (∼300 g) were anesthetized using a 0.7-mL i.p. injection of pentobarbital sodium (200 mg/mL Euthatal, Merial, UK). The beating hearts were removed quickly and arrested in ice-cold Krebs–Henseleit buffer (KHB, Sigma-Aldrich, UK), and the aorta was cannulated for perfusion in recirculating retrograde Langendorff mode (15 mL/min) at a constant 85 mmHg pressure and 37 °C. KHB solution was supplemented with 11 mM glucose and 0.6 mM Na-pyruvate.

The development of intraventricular pressure resulting from Thebesian artery drainage was minimized by the insertion of polyethylene tubing through the apex of the heart. End diastolic pressure was set to ∼6 mmHg. Heart rate and left ventricular systolic and diastolic pressure were recorded continuously using a PowerLab/4SP data acquisition system (ADInstruments Ltd). The perfused heart was placed in a 20-mm NMR sample tube and positioned inside the bore of an 11.7-T Bruker spectrometer (500 MHz for ^{1}H resonances; Bruker Biospin). The function of each heart was allowed to stabilize in the bore of the magnet while the heart was imaged to localize it in the center of the rf coils, and a slice-selective shim was implemented to reduce ^{1}H line width to ∼50 Hz.

Hyperpolarized ^{13}C magnetic resonance spectroscopy in perfused hearts. [1-^{13}C]Pyruvate for ex vivo experiments was prepared as described above but was polarized in a HyperSense ^{13}C polarizer system (Oxford Instruments) (4). Upon dissolution, 6 mL of hyperpolarized tracer (20 mM Na-pyruvate, pH 7.4, temperature ∼40 °C) was infused directly into 190 mL of oxygenated KHB + glucose (pyruvate-free), in a water-jacketed reservoir at 37 °C. Where indicated, inhibitors 4-(2,4,6-trimethylpyridinium-*N*-methylcarboxamido)-benzenesulfonamide perchlorate (C23), acetazolamide (ATZ), and 4,4'-diisothiocyanatostilbene-2,2'-disulfonic acid (DIDS) were added to this perfusate. After dissolution of hyperpolarized [1-^{13}C]pyruvate, pyruvate in the buffer was 0.6 mM. Acquisition of ^{13}C MR spectra commenced immediately after infusion of hyperpolarized [1-^{13}C]pyruvate, and infusion continued throughout acquisition. Spectra were acquired with 1-s temporal resolution over 2 min (30° excitation flip angle, 120 acquisitions). Spectra were centered at 125 ppm and referenced to the [1-^{13}C]pyruvate resonance at 171 ppm, and 4,096 points were acquired over a bandwidth of 180 ppm.

$H^{13}CO_3^-$ quenching protocol in perfused hearts. Two sequential experiments then were performed in each perfused heart:

i) Control: Hyperpolarized [1-^{13}C]pyruvate was diluted to 0.6 mM and perfused into the heart, and ^{13}C metabolites were detected with 1-s temporal resolution over the course of 2 min (30° excitation flip angle, 120 acquisitions, 180 ppm sweep width; 4,096 acquired points; frequency centered at 125 ppm). The precise frequency of the ^{13}C-bicarbonate resonance was noted.

ii) HCO_3^- saturation*:* After a second dose of [1-^{13}C]pyruvate was polarized (45 min), 0.6 mM [1-^{13}C]pyruvate again was delivered to the heart, and ^{13}C spectra were acquired as before while rf saturation was applied at 20-s intervals exactly at the $H^{13}CO_3^-$ resonance. To achieve the continuous saturation at the appropriate resonance frequency, a cascade of eight repeated SNEEZE pulses (5, 6) was applied. Each SNEEZE pulse had a time-bandwidth product of 5.82 and 100-ms duration, with 100-μs intervals between pulses. No saturation was applied during signal acquisition (180 μs). The effective FWHM bandwidth was ∼160 Hz when tested on a sample of acetone.

^{31}P magnetic resonance spectroscopy in perfused hearts. Initially, an unsaturated ^{31}P MR spectrum was acquired at 202.5 MHz from the hearts using a 90° pulse with repetition time of 15 s and 40 transients. Dynamic ^{31}P MR spectra were acquired using a 30° rf pulse and a repetition delay of 0.25 s throughout the protocol. Each spectrum consisted of 120 transients, giving a total acquisition time of 30 s. The unsaturated spectra were used to correct metabolite concentrations for the effects of saturation.

Analysis of Magnetic Resonance Spectroscopy Data. ***^{13}C.*** Cardiac ^{13}C MR spectra were analyzed using the AMARES algorithm, as implemented in the jMRUI software package (7). Spectra were corrected for DC offset based on the last half of acquired points, and peaks corresponding with [1-^{13}C]pyruvate and its metabolic derivatives were fitted assuming a Lorentzian line shape and initial peak frequencies, relative phases, and line widths. For spectra acquired in vivo, the maximum peak area of each metabolite over the acquisition was determined for each series of spectra and expressed as a ratio normalized to the maximum [1-^{13}C]pyruvate resonance (3). The rate of signal production for each metabolite, in arbitrary units (a.u.) per second, was measured as the slope of the mean metabolite increase over the first 5 s following its appearance, during which time the metabolite signal increased linearly.

^{31}P. Cardiac ^{31}P MR spectra were analyzed using the AMARES algorithm in the jMRUI software package (7). Spectra were corrected for DC offset using the last half of acquired points. The phosphocreatine (PCr) resonance was set at 0 ppm, and the chemical shifts of all peaks were referenced to that of PCr. The PCr, P_i, and γ-ATP resonances were fitted assuming a Lorentzian line shape, peak frequencies, relative phases, line widths, and J-coupling parameters.

SI Computational Methods

Determining Carbonic Anhydrase Activity from pH Time Courses Measured in Lysates. Lysate carbonic anhydrase (CA) activity was determined by best-fitting the experimental time course of medium acidification upon CO_2 addition (at 4 °C) with a mathematical model (8) formulated below:

$$\frac{\mathrm{dpH}}{\mathrm{dt}} = -\frac{\mathrm{CA}\cdot\left(\mathrm{k_h}\cdot[\mathrm{CO_2}] - \mathrm{k_r}\cdot[\mathrm{HCO_3^-}]\cdot 10^{-\mathrm{pH}}\right)}{\beta_{\mathrm{HepesMes}}(\mathrm{pH})}.$$

CA, the fitting variable, is the dimensionless index of CA activity. k_h and k_r are the uncatalyzed hydration and reverse (dehydration) rate constants at 4 °C, determined experimentally in 100 μM ATZ (under the constraint that ratio k_r/k_h equals the acid-dissociation constant K_a of CO_2/HCO_3^-; $10^{-6.38}$ M at 4 °C) (8). After the addition of CO_2-saturated water to the lysate, the diluted Hepes and MES were each 13.3 mM. The mixture's non-CO_2 buffering capacity ($\beta_{\mathrm{HepesMes}}$) was derived from Hepes and MES K_a at 4 °C ($10^{-7.68}$ M and $10^{-6.27}$ M, respectively) (8). Initial $[HCO_3^-] = 0$. Initial pH = 8.0. Initial $[CO_2]$ (i.e., before hydration had begun) was determined by multiplying the pH drop (at steady state) by $\beta_{\mathrm{HepesMes}}$.

Determining CA Activity from pH Time Courses Measured in Isolated Myocytes. Intracellular CA activity in an isolated myocyte was measured experimentally from the intracellular pH (pH_i) change in response to the addition and removal of superfusate CO_2 at 37 °C. The best-fit CA activity was obtained by fitting experimental time courses with a mathematical model (8) of three differential equations:

$$\frac{\mathrm{dpH_i}}{\mathrm{dt}} = -\frac{\mathrm{CA}\cdot\left(\mathrm{k_h}\cdot[\mathrm{CO_2}]_\mathrm{i} - \mathrm{k_r}\cdot[\mathrm{HCO_3}]_\mathrm{i}\cdot 10^{-\mathrm{pH_i}}\right)}{\beta_{\mathrm{int}}(\mathrm{pH_i})},$$

$$\frac{\partial[\mathrm{HCO_3^-}]_\mathrm{i}}{\partial \mathrm{t}} = \mathrm{CA}\cdot\left(\mathrm{k_h}\cdot[\mathrm{CO_2}]_\mathrm{i} - \mathrm{k_r}\cdot[\mathrm{HCO_3^-}]_\mathrm{i}\cdot 10^{-\mathrm{pH_i}}\right), \text{ and}$$

$$\frac{\partial[\mathrm{CO_2}]_\mathrm{i}}{\partial \mathrm{t}} = \mathrm{CA}\cdot\left(\mathrm{k_r}\cdot[\mathrm{HCO_3^-}]_\mathrm{i}\cdot 10^{-\mathrm{pH_i}} - \mathrm{k_h}\cdot[\mathrm{CO_2}]_\mathrm{i}\right) + \mathrm{P_{CO_2}}\cdot\mathrm{s}\cdot\left([\mathrm{CO_2}]_\mathrm{o}(\mathrm{t}) - [\mathrm{CO_2}]_\mathrm{i}\right)$$

CA, the fitting variable, is the dimensionless index of CA activity. k_h and k_r are the uncatalyzed hydration and reverse (dehydration) rate constants at 37 °C, determined experimentally in 100 μM ATZ ($k_r/k_h = 10^{-6.15}$ M at 37 °C) (9). Intrinsic buffering capacity (β_{int}) was determined previously (10). Membrane CO_2 permeability was set to 10^4 μm/s (11). The myocytes's surface area/volume ratio (s) was 0.5 μm^{-1} (12). Extracellular $[CO_2]$ ($[CO_2]_o$) was changed from 0 to 1.2 mM (and back) at an exchange time constant of 2.7 s (Fig. S3*B*). Starting pH_i was determined from the experiment.

Determining CA Activity from ^{13}C Signals in Intact Hearts. A system of ordinary differential equations (published previously in ref. 13) simulated the time course of unlabeled and hyperpolarized (denoted by *) [1-^{13}C]pyruvate (pyr), $^{13}CO_2$, and $H^{13}CO_3^-$:

$$\frac{\mathrm{d}[\mathrm{pyr}]_\mathrm{i}}{\mathrm{dt}} = \mathrm{P_{pyr}}\cdot\mathrm{s}\cdot\left([\mathrm{pyr}]_\mathrm{o} - [\mathrm{pyr}]_\mathrm{i}\right) - \rho\cdot[\mathrm{pyr}]_\mathrm{i} + \lambda_{\mathrm{pyr}}\cdot[\mathrm{pyr}]_\mathrm{i}$$

$$\frac{\mathrm{d}[\mathrm{pyr}*]_\mathrm{i}}{\mathrm{dt}} = \mathrm{P_{pyr}}\cdot\mathrm{s}\cdot\left([\mathrm{pyr}*]_\mathrm{o} - [\mathrm{pyr}*]_\mathrm{i}\right) - \rho\cdot[\mathrm{pyr}*]_\mathrm{i} - \lambda_{\mathrm{pyr}}\cdot[\mathrm{pyr}*]_\mathrm{i}$$

$$\begin{aligned}\frac{\mathrm{d}[\mathrm{CO_2}]_\mathrm{i}}{\mathrm{dt}} = {} & \mathrm{P_{CO_2}}\cdot\mathrm{s}\cdot\left([\mathrm{CO_2}]_\mathrm{o} - [\mathrm{CO_2}]_\mathrm{i}\right) \\ & + \mathrm{CA}\cdot\left(\mathrm{k_r}\cdot[\mathrm{HCO_3^-}]_\mathrm{i}\cdot[\mathrm{H^+}]_\mathrm{i} - \mathrm{k_h}\cdot[\mathrm{CO_2}]_\mathrm{i}\right)\ldots \\ & + \rho\cdot\left(3\cdot[\mathrm{pyr}]_\mathrm{i} + 2\cdot[\mathrm{pyr}*]_\mathrm{i}\right) + \lambda_{\mathrm{CO2}}\cdot[\mathrm{CO_2}]_\mathrm{i}\end{aligned}$$

$$\begin{aligned}\frac{\mathrm{d}[\mathrm{CO_2}*]_\mathrm{i}}{\mathrm{dt}} = {} & \mathrm{P_{CO_2}}\cdot\mathrm{s}\cdot\left([\mathrm{CO_2}*]_\mathrm{o} - [\mathrm{CO_2}*]_\mathrm{i}\right) \\ & + \mathrm{CA}\cdot\left(\mathrm{k_r}\cdot[\mathrm{HCO_3^-}*]_\mathrm{i}\cdot[\mathrm{H^+}]_\mathrm{i} - \mathrm{k_h}\cdot[\mathrm{CO_2}*]_\mathrm{i}\right)\ldots \\ & + \rho\cdot[\mathrm{pyr}*]_\mathrm{i} - \lambda_{\mathrm{CO2}}\cdot[\mathrm{CO_2}*]_\mathrm{i}\end{aligned}$$

$$\frac{\mathrm{d}[\mathrm{HCO_3^-}]_\mathrm{i}}{\mathrm{dt}} = \mathrm{CA}\cdot\left(\mathrm{k_h}\cdot[\mathrm{CO_2}]_\mathrm{i} - \mathrm{k_r}\cdot[\mathrm{HCO_3^-}]_\mathrm{i}\cdot[\mathrm{H^+}]_\mathrm{i}\right) + \lambda_{\mathrm{HCO3}}\cdot[\mathrm{HCO_3^-}]_\mathrm{i}$$

$$\frac{\mathrm{d}[\mathrm{HCO_3^-}*]_\mathrm{i}}{\mathrm{dt}} = \mathrm{CA}\cdot\left(\mathrm{k_h}\cdot[\mathrm{CO_2}*]_\mathrm{i} - \mathrm{k_r}\cdot[\mathrm{HCO_3^-}*]_\mathrm{i}\cdot[\mathrm{H^+}]_\mathrm{i}\right) - \lambda_{\mathrm{HCO3}}\cdot[\mathrm{HCO_3^-}*]_\mathrm{i}$$

The following parameters were determined by best-fitting: ρ, a rate constant that approximated the kinetics of pyruvate respiration; λ, the decay constant describing the lifetime of hyperpolarized ^{13}C compounds in the intracellular space; k_h and k_r, the hydration and reverse (dehydration) reaction rate constants of the CO_2-HCO_3 equilibrium; *CA*, a scalar describing CA activity.

Subscripts *i* and *o* denote intra- and extracellular concentrations. Membrane permeability to pyruvate (P_{pyr}) and CO_2 (P_{CO2}) were set to 0.4 μm/s and 10^4 μm/s, respectively (11). The myocytes's surface area/volume ratio (s) was 0.5 μm^{-1} (12). Because of the high pH buffering capacity and the activity of pH_i-regulating proteins, pH_i was assumed to be constant. $[CO_2]_o$ and $[HCO_3]_o$ were set to their equilibrium concentrations of 1.2 mM and 22 mM, respectively. Assuming adequate capillary washout, initial $[CO_2*]_o$ and $[HCO_3*]_o$ were set to zero. Total extracellular pyruvate ($[pyr]_o$+ $[pyr*]_o$) was fixed to 2.5 mM, but $[pyr]_o$ and $[pyr*]_o$ varied with time, as described below assuming that 25% of pyruvate (i.e., 0.625 mM) is hyperpolarized at C^1:

$$[\mathrm{pyr}]_0 = \begin{cases} 2.5\ \mathrm{mM} & \mathrm{t} < 0 \\ 2.5 - (0.625\cdot\exp(-\alpha_\mathrm{E}\cdot\mathrm{t}))\ \mathrm{mM} & \mathrm{t} > 0; \end{cases}$$

$$[\mathrm{pyr}*]_0 = \begin{cases} 0\ \mathrm{mM} & \mathrm{t} < 0 \\ 0.625\cdot(\exp(-\alpha_\mathrm{E}\cdot\mathrm{t}))\ \mathrm{mM} & \mathrm{t} > 0. \end{cases}$$

1. Thomas JA, Buchsbaum RN, Zimniak A, Racker E (1979) Intracellular pH measurements in Ehrlich ascites tumor cells utilizing spectroscopic probes generated in situ. *Biochemistry* 18(11):2210–2218.
2. Xiong JW, Zhu L, Jiao X, Liu SS (2010) Evidence for DeltapH surface component (DeltapH(S)) of proton motive force in ATP synthesis of mitochondria. *Biochim Biophys Acta* 1800(3):213–222.
3. Schroeder MA, et al. (2008) In vivo assessment of pyruvate dehydrogenase flux in the heart using hyperpolarized carbon-13 magnetic resonance. *Proc Natl Acad Sci USA* 105(33):12051–12056.
4. Schroeder MA, et al. (2009) Real-time assessment of Krebs cycle metabolism using hyperpolarized 13C magnetic resonance spectroscopy. *FASEB J* 23(8):2529–2538.
5. Schroeder MA, et al. (2012) The cycling of acetyl-coenzyme A through acetylcarnitine buffers cardiac substrate supply: A hyperpolarized 13C magnetic resonance study. *Circ Cardiovas Imaging* 5(2):201–209.
6. Freeman R (1998) Shaped radiofrequency pulses in high resolution NMR. *Prog Nucl Magn Reson Spectrosc* 32(1):59–106.
7. Naressi A, Couturier C, Castang I, de Beer R, Graveron-Demilly D (2001) Java-based graphical user interface for MRUI, a software package for quantitation of in vivo/medical magnetic resonance spectroscopy signals. *Comput Biol Med* 31(4): 269–286.
8. Swietach P, et al. (2008) Tumor-associated carbonic anhydrase 9 spatially coordinates intracellular pH in three-dimensional multicellular growths. *J Biol Chem* 283(29): 20473–20483.
9. Leem CH, Vaughan-Jones RD (1998) Out-of-equilibrium pH transients in the guinea-pig ventricular myocyte. *J Physiol* 509(Pt 2):471–485.
10. Zaniboni M, et al. (2003) Intracellular proton mobility and buffering power in cardiac ventricular myocytes from rat, rabbit, and guinea pig. *Am J Physiol Heart Circ Physiol* 285(3):H1236–H1246.
11. Itel F, et al. (2012) CO2 permeability of cell membranes is regulated by membrane cholesterol and protein gas channels. *FASEB J* 26(12):5182–5191.
12. Satoh H, Delbridge LM, Blatter LA, Bers DM (1996) Surface:volume relationship in cardiac myocytes studied with confocal microscopy and membrane capacitance measurements: Species-dependence and developmental effects. *Biophys J* 70(3):1494–1504.
13. Schroeder MA, et al. (2010) Measuring intracellular pH in the heart using hyperpolarized carbon dioxide and bicarbonate: A 13C and 31P magnetic resonance spectroscopy study. *Cardiovasc Res* 86(1):82–91.

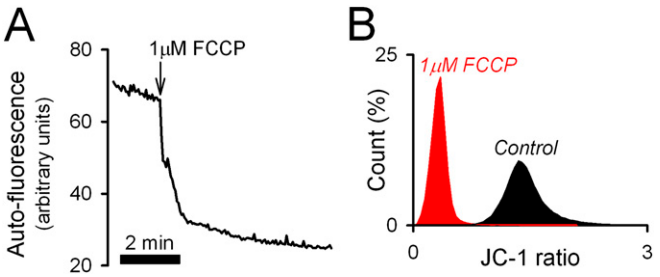

Fig. S1. Test of mitochondrial viability. (*A*) Fluorescence from mitochondria (suspended in mitochondrial storage buffer) measured using a cuvette spectrofluorometer. The addition of 1 μM FCCP (carbonyl cyanide-p-trifluoromethoxyphenylhydrazone) decreased signal, as expected from NADH depletion. (*B*) Mitochondrial membrane potential (ψ_m) measured flow cytometrically with the fluorescent dye JC-1: FCCP (1 μM) decreased the 525/580 nm ratio (depolarization).

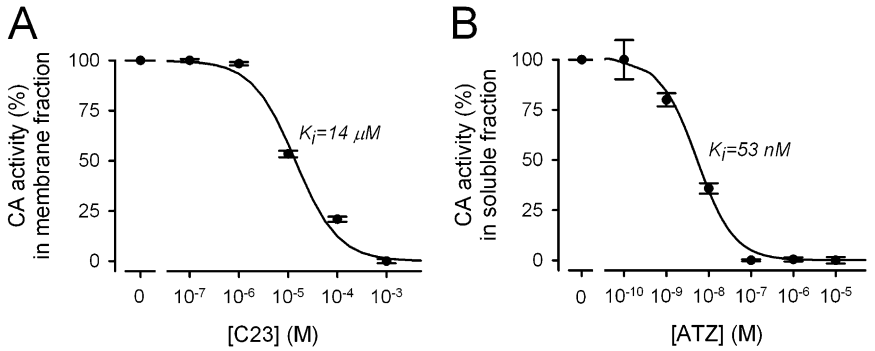

Fig. S2. Determination of drug-inhibition constants (K_i). (*A*) Dose–response curve for C23 [4-(2,4,6-trimethylpyridinium-*N*-methylcarboxamido)-benzene sulfonamide perchlorate], measured in the membrane fraction of whole-ventricle lysates obtained as the pellet following centrifugation at 9,000 rpm at 4 °C for 6 min, repeated once. CA activity measurements were performed at 4 °C according to the assay described in Fig. 1*A*. K_i (determined by best-fit to Hill curve) of 14 μM. (*B*) Dose–response curve for ATZ, measured in the soluble fraction of whole-ventricle lysates obtained as the supernatant following centrifugation at 9056 × *g* at 4 °C for 6 min. K_i of 53 nM.

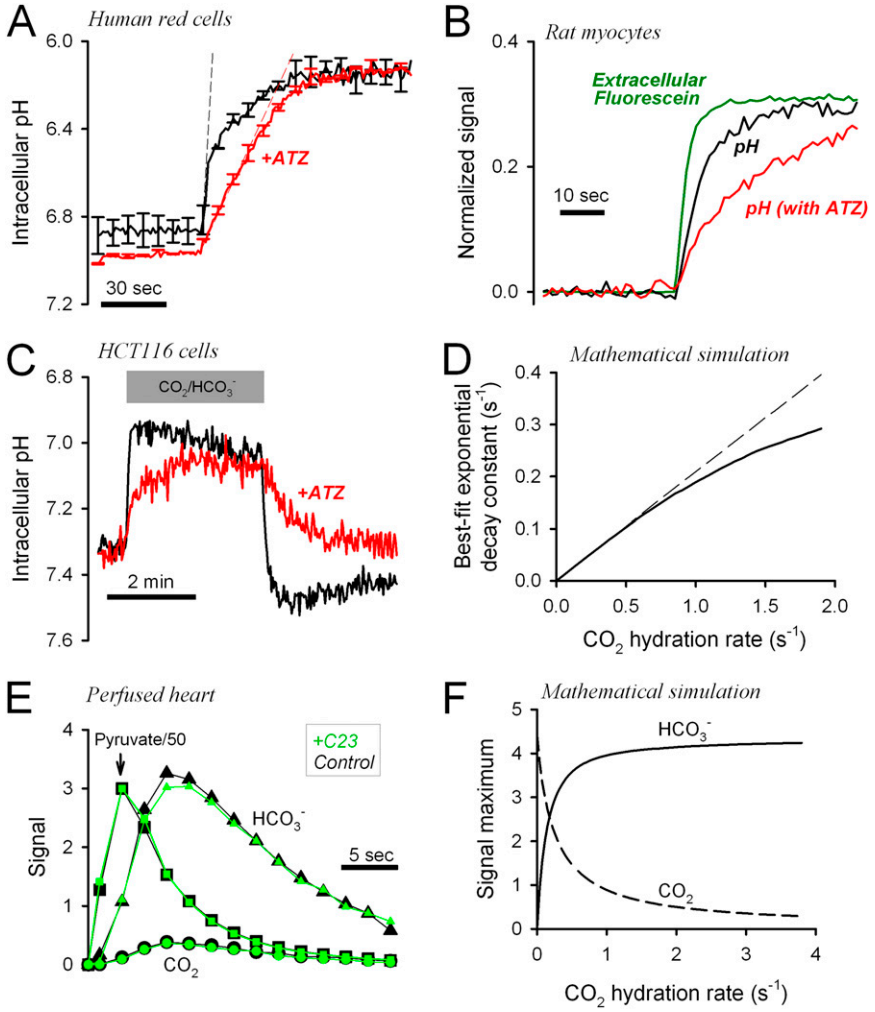

Fig. S3. Validation of the addition of extracellular CO_2 as a method for measuring CA activity and further experiments and analyses of hyperpolarized $^{13}CO_2$ hydration. (*A*) Measurement of CA activity in BCECF-loaded human red cells (obtained from P.S.) following the protocol described in Fig. 1*B* ($n = 3$). The ability of the assay to detect CA activity is confirmed by the substantial slowing of CO_2-evoked acidification in the presence of 100 μM ATZ. (*B*) Superfusion experiments performed on isolated rat ventricular myocytes. pH_i changes (measured with cSNARF-1) evoked by the addition of CO_2 in the presence (red) and absence (black) of 100 μM ATZ (data from Fig. 2A). The kinetics of these responses (control time constant, 8 s) were not rate-limited by the much faster solution exchange determined in separate experiments using superfusates containing 30 μM fluorescein ($n = 10$; time constant 2.7 s; green trace). (*C*) Superfusion experiments performed on colon cancer-derived HCT116 cells (cultured to 70–90% confluency) using the protocol shown in Fig. 2*A*. Total intracellular CA activity in this cell type catalyzes CO_2 hydration sevenfold, indicating that the 2.7-fold CA activity measured in ventricular myocytes (Fig. 2*A*) is not at saturation of the method's resolving power. (*D*) Mathematical simulation (*SI Computational Methods*) of the relationship between the intracellular CO_2 hydration rate constant (proportional to CA activity) and the best-fit exponential decay constant for the resulting pH_i time course, assuming a time constant for solution exchange of 2.7 s (if the solution exchange were instantaneous, a linear relationship would be expected). The simulated curve is linear for $0 < k_h < 0.78$.s (CA activities of up to ~fourfold), beyond which the method introduces an error because solution exchange becomes a rate-limiting factor. (*E*) C23 (2 μmol infused to animal) did not affect the time course of ^{13}C-labeled metabolites following [1-^{13}C]pyruvate infusion into rats in vivo ($n = 7$; error bars not shown for clarity). (*F*) Mathematical simulation of the relationship between CO_2 hydration rate and peak $H^{13}CO_3^-$ and peak $^{13}CO_2$ during [1-^{13}C]pyruvate infusion. The model is based on the equations presented in *SI Computational Methods*. The ratio of peak $^{13}CO_2$ signal to peak $H^{13}CO_3^-$ signal provides a measure of CA activity in the volume containing $^{13}CO_2$.

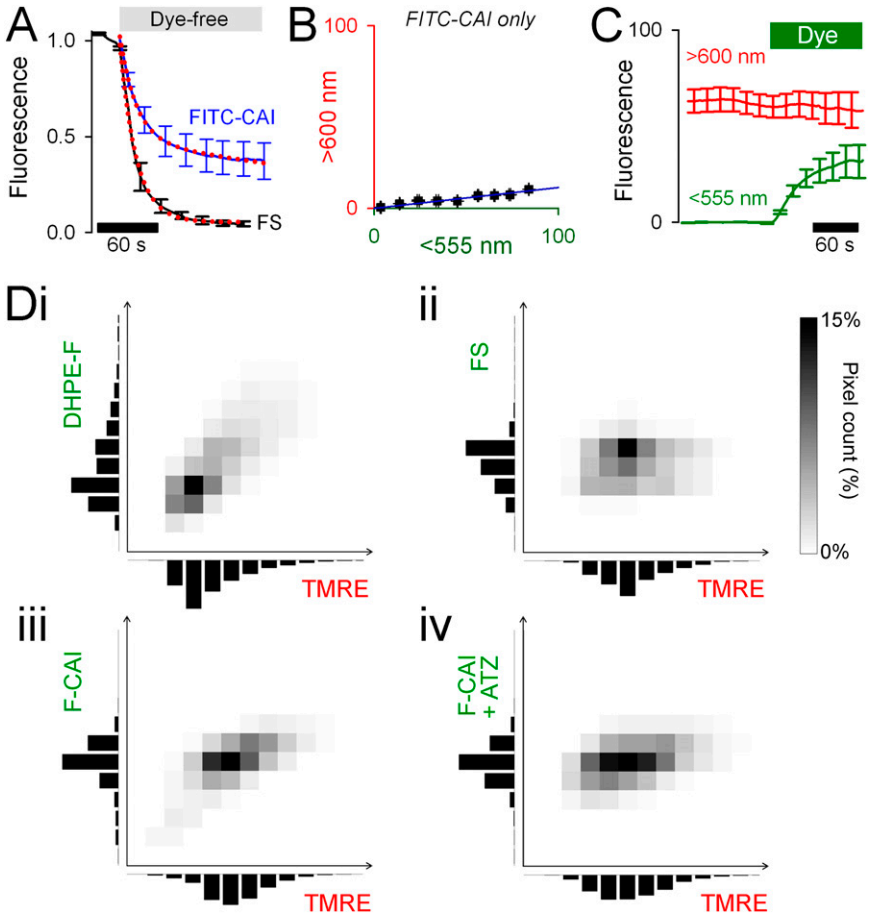

Fig. S4. Colocalization of fluorescein-derivatives with mitochondria (labelled with the marker TMRE). (*A*) Fluorescence (excited at 488 nm) in permeabilized myocytes during washout of 1mM fluorescein sulfonate (FS) or fluorescein-conjugated CA inhibitor (F-CAI). Best-fit time constants were15 s and 480 s, respectively. (*B*) F-CAI fluorescence bleed-through to >600 nm (i.e., TMRE detection range) was 11%. (*C*) Exposure to F-CAI did not alter TMRE fluorescence, indicating that the spatial separation between the fluorophores is outside the range for FRET. (*D*) Pixel-by-pixel relationship between fluorescence emitted by TMRE and fluorescein derivatives. 2D histogram analysis showing correlation between TMRE fluorescence and (*i*) membrane-tagging DHPE-F (positive control), (*ii*) membrane-impermeant FS (negative control), (*iii*) F-CAI, and (*iv*) F-CAI in the presence of the nonfluorescent competitor 1 mM ATZ.

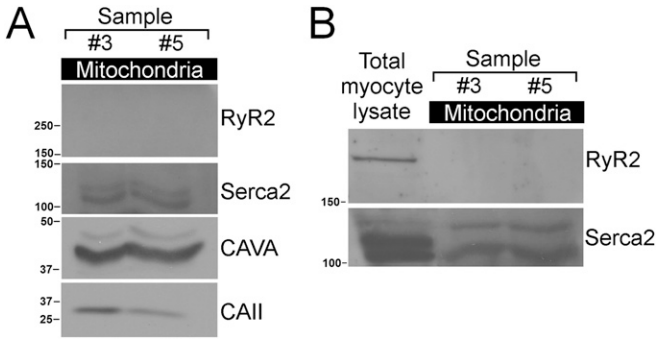

Fig. S5. Western blot analysis of cardiac mitochondria. (*A*) Sample number indicates the number of washes performed to purify mitochondria. Samples were negative for ryanodine receptor type 2 (RyR2) [associated with junctional sarcoplasmic reticulum (SR)] and positive for sarcoplasmic reticulum Ca^{2+} ATPase 2a (SERCA2) (associated with network SR) and CAVA (a marker of mitochondria). CAII immunoreactivity was detected even after five consecutive washes. (*B*) Total myocyte lysates were tested positive for RyR2 and SERCA2. Mitochondrial fractions were positive for SERCA2 but not for RyR2, indicating that fragments of network SR associate with the mitochondria.

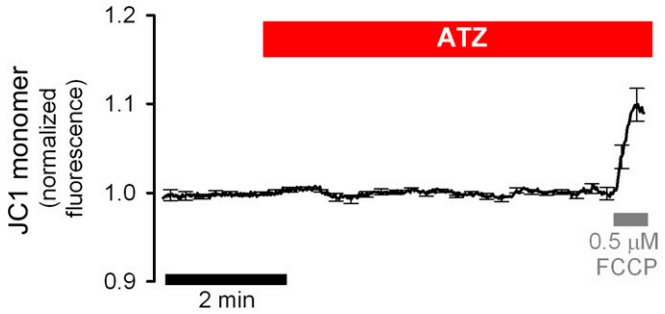

Fig. S6. Effect of ATZ on mitochondrial membrane potential (ψ_m). Permeabilized rat ventricular myocyte, loaded with the ψ_m reporter JC-1 (5 μM). ATZ (100 μM) did not alter ψ_m. FCCP depolarized ψ_m. Superfusion in mitochondrial respiration buffer.

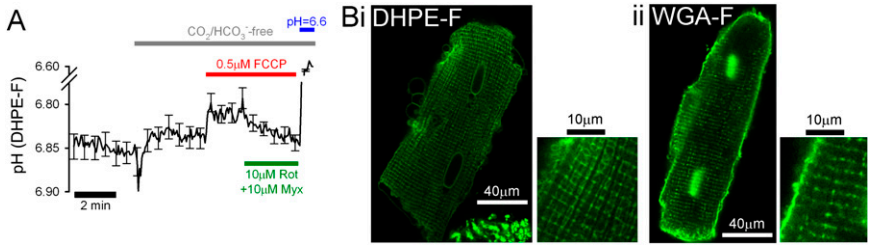

Fig. S7. Validation of method to measure inter-membrane space (IMS) pH using DHPE-fluorescein (DHPE-F). (*A*) Permeabilized rat ventricular myocytes ($n = 8$) were treated with DHPE-F for 10 min before superfusion with mitochondrial respiration buffer containing CO_2/HCO_3^- (pH 7.0). The switch to CO_2/HCO_3^--free buffer evoked a transient alkaline response (indicative of a weakly buffered space in which pH is being measured). Sustained acidification upon exposure to FCCP and recovery following inhibition of complexes I and III with myxothiazol (Myx) and rotenone (Rot), respectively, are characteristic of the pH response in the IMS. Calibration was with Hepes-buffered internal solution at pH = 6.6. (*B*) Confocal images (100×) of (*i*) a myocyte treated with DHPE-F, showing staining of the mitochondrial boundaries, and (*ii*) a myocyte treated with wheat germ agglutinin-conjugated fluorescein (WGA-F), showing staining the sarcolemma, T system, and nuclei.

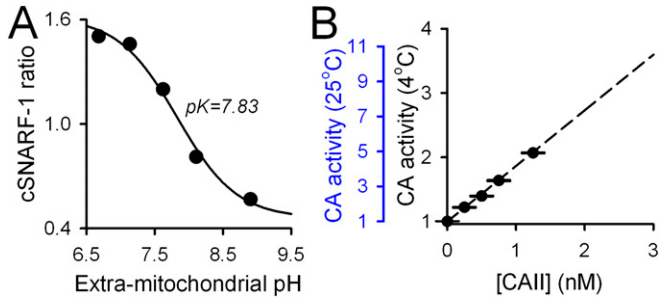

Fig. S8. (*A*) Calibration curve for mitochondria-loaded cSNARF-1, measured by flow cytometry. Mitochondria were suspended in high K^+ solutions (at pH 6.7, 7.1, 7.6, 8.1, or 8.9) containing 5 μM nigericin and 1 μM FCCP. (*B*) Conversion of CAII concentration to CA activity (from the rate of pH change upon CO_2 addition, a method similar to that shown in Fig. 1*A*) measured at 4 °C and extrapolated to 25 °C (based on ref. 1).

1. Forster RE (1991) Methods for the measurement of carbonic anhydrase activity. *The Carbonic Anhydrases: Cellular Physiology and Molecular Genetics* ed Dodgson SJ, Plenum, New York).

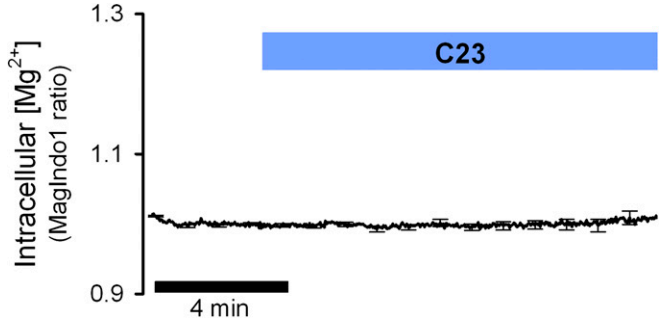

Fig. S9. Effect of C23 on intracellular $[Mg^{2+}]$. Intact rat ventricular myocyte was loaded with the $[Mg^{2+}]$ reporter dye Mag-Indo-1. Superfusion in 5% CO_2/HCO_3^--buffered NT. Exposure to C23 (15 μM) did not alter intracellular $[Mg^{2+}]$.